IEEE *Access*
Multidisciplinary : Rapid Review : Open Access Journal

A Novel High-Efficiency S-Band Conical Axial Vircator

P. LIVRERI[1] (Senior Member, IEEE)
[1]Department of Engineering, University of Palermo, Palermo, IT 90133

Corresponding authors: P. Livreri (e-mail: patrizia.livreri@unipa.it)

ABSTRACT A VIRtual CAThode oscillatOR (Vircator) is a High-Power Microwave (HPM) vacuum electron device (VED) with applications in the field of health, energy, space, environment, and defense. In this work, a novel high efficiency S-band Vircator for counter Ummanned Aerial Vehicle (UAV) is presented. At first, starting from the geometrical and physical parameter values chosen, an axial vircator is designed. Then, to enhance its efficiency, a conical structure is added into the cylindric waveguide, altering the electron beam dynamic and optimizing the interaction with the virtual cathode. The Particle-in-Cell simulation carried out by CST Studio suite 2024, shows an average output power of $50\,\mathrm{MW}$ and an efficiency up to $60\,\%$ than the classic geometry ones, with an applied voltage of $520\,\mathrm{kV}$ and a cathode current of $20\,\mathrm{kA}$ at $2.55\,\mathrm{GHz}$.

INDEX TERMS Vircator, High Power Microwave, Microwave source, Oscillator, High-efficiency, Axial configuration, Conical configuration.

I. INTRODUCTION

High power microwaves (HPMs) are defined as electron devices operating between 1 and $300\,\mathrm{GHz}$ with an output peak power of up to 100 MW, aiming to intentionally disturb or destroy electronic equipments without damaging infrastructure or injuring people [1]. The schematic block diagram of a complete HPM system is shown in Figure 1. It is composed of a Pulse Power Source, a High Power Microwave source, and an antenna. The pulse power source is, generally, a Marx generator and consists of an array of capacitors which are charged in parallel and discharged in series to generate high voltage pulses. The High Power Microwave (HPM) source is a vacuum electron device (VED) such as a Virtual Cathode Oscillator, Vircator, or a Magnetically Insulated Line Oscillator, Milo. Generally, a Vircator is used for its simple fabrication as it requires no external magnetic field and exhibits a low impedance value [2]–[12]. The antenna is, generally, a flared horn through which the generated microwave power is emitted to the free-space. Vlasov antennas and their geometrical modifications have been largely investigated to guarantee a wider emission angle [13]. The three most common geometries adopted to design the vircator are the axial, coaxial, and reflex triode [14]–[16]. The axial vircator without an external magnetic field, is largely used for its simplicity and low-weight. Despite its simplicity of construction, the Vircator provides an efficiency less than $2\,\%$.

In literature, several techniques have been proposed to increase the energy conversion efficiency of the standard axial mode. In [17], a comprehensive state of the art of all the published geometries with their efficiency value is reported. In particular, a pinch-vircator providing an efficiency $11\,\%$ is designed in [11], [12] based to the concept that pinching of the beam increases the electron density near the VC and prevents the escape of drifting electrons and the early deposition of the electrons on the walls. A multibeam scheme is proposed in [18] consisting of several electron beams with supercritical currents charged onto a common resonator. This can be achieved by using a relativistic electron beam with the highest current of the beam determining the frequency and the remaining $(N - 1)$ beams with lower currents as supporting beams, which "pump" the required energy into the system. The multibeam architecture is not affected by bandwidth reduction. A multistage architecture is proposed in [19], based on the formation of virtual cathodes (VCs) generated by thin metallic anodic foils, called reflectors, inside the drift tube. A second virtual cathode (VC2) is generated by forcing the drifting electrons from traditional VC1 as a wall charge accumulated at a floating zone plate [20]. In [21], multi virtual cathodes (MVCs) were created in an axial vircator utilizing two dielectric reflectors (DRs) improving the efficiency from $7.9\,\%$ to $28.6\,\%$. In [22], an optimization in terms of both reflectors radii and distances for a multi-stage

axial Vircator able to provide an efficiency up to 15.6% is presented.

In this work, a novel high-efficiency axial vircator based on a conic structure added to the circular waveguide, is proposed. This article is organized as follows. In Section II, the vircator operating principle is described. The design and Particle-in-Cell simulation for an axial vircator are reported in Section III. In Section IV, the novel conical axial vircator geometry is described and the simulation results are reported. Finally, in Section V, conclusions are given.
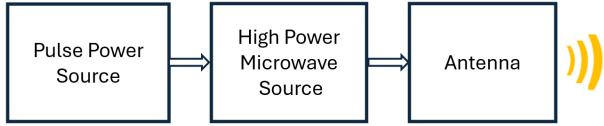

FIGURE 1. High Power Microwave (HPM) schematic block system.

II. VIRCATOR OPERATING PRINCIPLE

The schematic model of an axial Virtual Cathode Oscillator without electromagnetic field is shown in Figure 2. Electrons emitted from the cathode are accelerated by the semitransparent anode and pass through it. At a distance from the anode of approximately the cathode-anode gap distance, the space charge limit is reached and a cloud of electrons forms the virtual cathode. When the virtual cathode is formed, it occurs that:

a) the virtual cathode begins to approach the anode until the kinetic energy of electrons is sufficient to pass through the virtual cathode and the virtual cathode dissolves. When the electron beam exceeds its space-charge limit current again, a new virtual cathode is formed. This periodic formation of virtual cathodes creates an oscillation that generates an electromagnetic radiation f_{vc} approximately at the plasma frequency f_p;

b) some electrons pass through the virtual cathode and other ones are reflected. The electrons with negative impulse are those reflected by the virtual cathode. These electrons will also oscillate between the cathode and the virtual cathode at a frequency f_r. If these two phenomena are forced to oscillate at the same frequency, by means of resonant cavities, better performance for the vircator can be obtained.

The drifting electrons are responsible of the low vircator efficiency [23]. In the axial vircator, the radiation of the space-charge cloud couples to radial and longitudinal electric field components of characteristic TM electromagnetic modes of a cylindrical cavity that are extracted through the cylindrical waveguide [24].

In the Vircator, the virtual cathode formed after the transparent anode oscillates with, approximately, the plasma frequency, f_p given by [25]

$$f_p = \frac{1}{2\pi} \sqrt{\frac{\rho e^2}{\epsilon_0 \gamma m}} \tag{1}$$

where ρ is the injected electron density, e the electron charge 1.602×10^{-19} C, ϵ_0 the permittivity of free space, m the rest mass of an electron $9.1093837015 \times 10^{-31}$ kg, and γ the relativistic factor.

The relativistic factor γ, by assuming that the real and virtual cathodes are equidistant from the anode, is calculated as [26]:
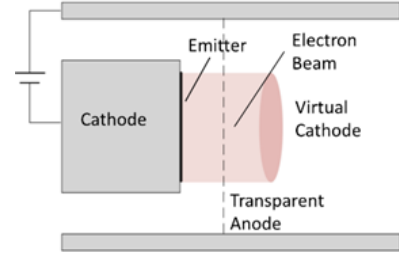

FIGURE 2. Schematic of an axial Virtual Cathode Oscillator.

$$\gamma = \sqrt{\frac{1}{1 - \left(\frac{v}{c}\right)^2}} \tag{2}$$

where c is the speed of light 3×10^8 m s and v is the electrons speed given by:

$$v = c \sqrt{1 - \frac{1}{\left[1 + \left(\frac{eV_0}{mc^2}\right)\right]^2}} \tag{3}$$

with V_0 the applied voltage over the anode-cathode gap distance.

The operating frequency of the virtual cathode f_{vc} is related to the plasma frequency f_p as $f_p \leq f_{vc} \leq (2\pi)^{\frac{1}{2}} f_p$ [23], [24].

For an axial vircator, f_{vc} is given by [26]:

$$f_{vc} = \frac{4.77}{d_{AK}} \ln \left(\gamma + \sqrt{\gamma^2 - 1} \right) \tag{4}$$

where d_{AK} is the anode to cathode distance.

The reflected electrons of the virtual cathode oscillate at a frequency f_r given by:

$$f_r = \frac{1}{4\tau_{AK}} \tag{5}$$

with τ_{AK} the transit time for electrons to travel from the cathode to the anode.

τ_{AK} can be expressed in terms of the distance d_{AK} and the electron velocity v as:

$$\tau_{AK} = \frac{d_{AK}}{\sqrt{V_0}} \cdot \sqrt{\frac{2mc^2 + eV_0}{ec^2}} \tag{6}$$

So, it occurs:

$$f_r = \frac{\sqrt{v_0}}{4d_{AK}} \sqrt{\frac{ec^2}{2mc^2 + eV_0}} \tag{7}$$

IEEE *Access*

III. DESIGN AND PARTICLE-IN-CELL SIMULATION FOR A CLASSIC AXIAL VIRCATOR

The design of the S-band Vircator starts with a classical axial configuration modeled by CST studio 2024 using its mesh generator module. In Figure 3, the 3D CST schematic model of the axial vircator is shown.

Starting from Eq. 7, physical parameters are obtained by plotting a graphical chart with the anode-cathode distance d_{AK} vs input voltage V_0 with the frequency f_r as a parameter.

For an operating frequency of 2.55 GHz, a cathode voltage equal to $520 \, \mathrm{kV}$ and an anode-to-cathode distance d_{AK} equal to $2.45 \, \mathrm{cm}$ are obtained from the graphical chart.

FIGURE 3. 3D CST schematic model of the axial vircator.

For the cathode, an emission surface with a radius $r_c = 4.6 \, \mathrm{cm}$ and a length equal to $6 \, \mathrm{cm}$ are considered.

The maximum current density can be derived from the Child-Langmuir law of a planar diode, given by:

$$J_{scl} = 2.33 \times 10^{-6} \frac{V_0^{3/2}}{d_{AK}^2} \qquad (8)$$

The space charge limiting current for a cylindrical electron beam can be expressed as [9]:

$$I_{scl} = J_{scl} \times S \qquad (9)$$

where S is the cathode surface given by πr_c^2 being r_c the cathode radius.

The space charge limiting current corresponding to the chosen cathode radius is equal to $I_{scl} = 9.3 \, \mathrm{kA}$.

If one-dimensional electron flow is considered, then the beam radius r_b and the cathode beam r_c can assume the same value.

The radius of the waveguide r_g is chosen according to the relationship:

$$f_{01} < f_{vc} < f_{02} \qquad (10)$$

where f_{01} ed f_{02} are the cut-off frequencies for TM_{01} and TM_{02} modes, respectively, given by:

$$(f_{cut-off})_{0n}^{TM} = \frac{p_{0n} \cdot c}{2\pi r_g} \qquad (11)$$

where c is the light speed and p_{0n} are the *0n-zero* of the Bessel function equal to 2.045 and 5.520 for TM_{01} e TM_{02} modes, respectively.

Being f_{01} and f_{02} equal to 1.43 GHz and 3.29 GHz, respectively, r_g is fixed equal to 7.6 cm to reject higher order modes and have single-mode propagation. The length of the circular

guide is chosen equal to $60 \, \mathrm{cm}$. This value should allow for better propagation of the TM_{01} mode and a significant increase in power through the tube [21].

The vircator design takes into consideration the physical and geometric parameters $f_p, f_{vc}, f_r, V_0, d_{AK}, r_c, r_g$, and their relationships, resulting in a complex and time-consuming method. The simulation physical and geometrical parameters for the axial vircator are reported in Table I.

TABLE I. Physical and geometrical parameters for the axial S-band vircator

Parameter	Quantity	Dimension
Operating frequency	2.55	GHz
Cathode Voltage	520	kV
Beam Current	20	kA
Cathode-anode distance	2.45	cm
Axial and radial grid width	4.5	mm
Guide radius	7.6	cm
Cathode radius	4.6	cm
Length of the guide	60	cm
Length of the cathode	6	cm

The axial vircator is fed by a $520 \, \mathrm{kV}$ pulsed voltage with rise time of $5 \, \mathrm{ns}$ and a pulse duration of $50 \, \mathrm{ns}$. In Figure 4, the waveform of the applied voltage pulse normalized to $520 \, \mathrm{kV}$ is shown.
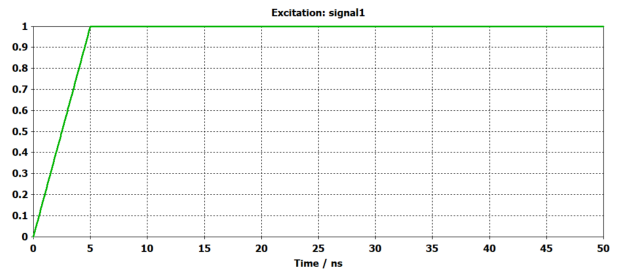

FIGURE 4. Applied voltage pulse normalized to 520 kV.

The cathode emission process is controlled by an explosive emission model, with a $100 \, \mathrm{kV/m}$ threshold value. The virtual cathode (VK) is formed at a distance from the real cathode of the order of twice the anode to cathode (AK) ones, as shown in Figure 5.
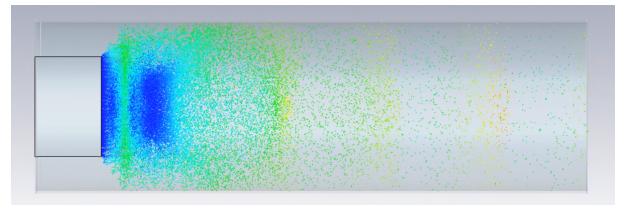

FIGURE 5. Electron charge distribution with the virtual cathode.

During the VK formation process, the electromagnetic field of oscillating electrons couples the EM fields of the waveguide modes. After the VK formation, electrons get

bunched in the downstream region of the waveguide, as shown in Figure 6. In Figure 7, the simulated instantaneous total output power for the classic axial vircator is shown.
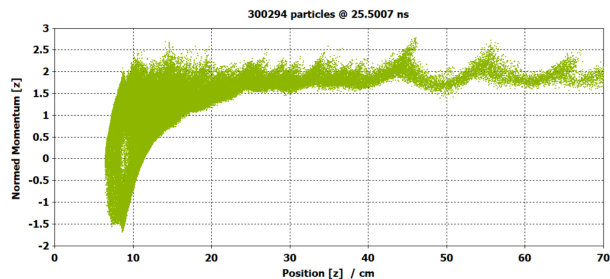

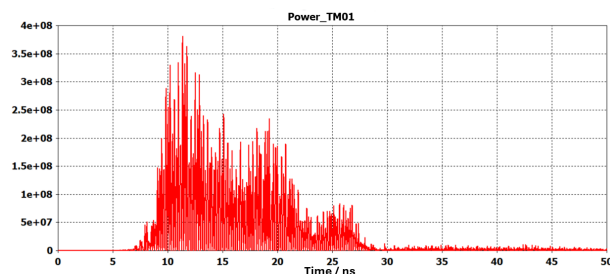**FIGURE 6.** Normalized momentum for classic axial Vircator.

FIGURE 7. Output peak power vs time for the classic axial vircator.

Figure 8 shows the Fourier spectrum for the classic axial vircator. The total output power is entirely supported by the TM_{01} mode at a frequency equal to 2.55 GHz.
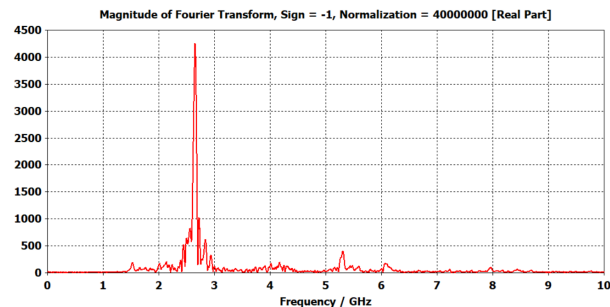

FIGURE 8. Fourier spectrum for the classic axial vircator.

Figure 9 shows the output peak power of the TE_{11} mode for the classic axial vircator.

Figure 10 shows the wave particle transfer for the classic vircator geometry.

IV. NOVEL CONICAL AXIAL VIRCATOR

Figure 11 shows the schematic model of the proposed novel conical axial vircator. It consists of a classic axial Vircator configuration with two conical metal "slices" inserted in the cylindrical waveguide which make the exit barrel-shaped.

The fundamental principle behind the proposed novel geometry is to increase the electric field intensity related to
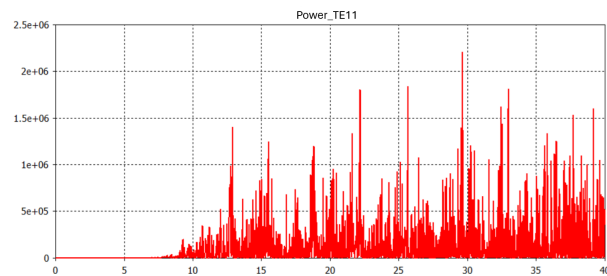

FIGURE 9. Output peak power vs. time for the TE_{11} mode of the classic axial vircator.
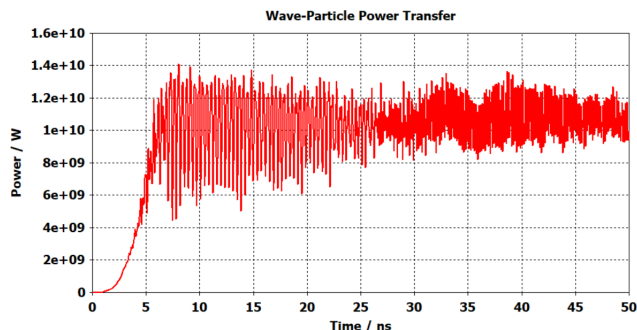

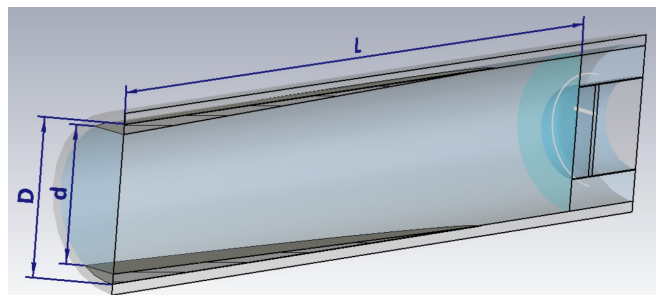**FIGURE 10.** Wave particle transfer for the classic axial vircator configuration.

FIGURE 11. CST schematic model of the novel conical axial Vircator geometry.

the TM_{01} mode. According to Poynting's theorem [27], since the cross-sectional area gradually narrows, it follows that the vector $E \times H$ increases, being E the electric and H the magnetic field, respectively. However, this increase has a limit beyond which the triggering of other modes drains energy from the TM_{01} mode.

The increase in the electric field relative to the TM_{01} mode enhances the interaction with the virtual cathode, consequently increasing the energy flux within the Vircator. This enhanced interaction is crucial for achieving higher efficiency and power output, as demonstrated by the simulation results.

In the proposed conical axial Vircator design, the gradual narrowing of the cross-sectional area results in an increase in the electric field intensity for the TM_{01} mode. This intensified electric field enhances the interaction with the virtual cathode, leading to a more efficient energy transfer and microwave generation process [28], [29].

IEEE *Access*

The analysis of this structure is carried out starting from the design of the classical axial cylindrical waveguide with an aperture of the two slides equal to zero. The performance of the conical axial vircator, in terms of spectral purity, output power, and energy contained in the pulse, are analyzed and optimized by varying the aperture of the added cone "slices" for the different propagation modes that can be triggered in the device.

Figure 12 shows the parametric analysis of the average output power vs the half-height of the exit window (corresponding to the aperture of the cone-slice) for the fundamental mode TM_{01} by varying the aperture and therefore the width of the output window. Different half-height of the output window, corresponding to a variation in terms of conical angles, have been considered and simulated to obtain the optimum value of output window corresponding to the optimum angle. The optimum value in terms of high average power has been obtained at 4.6 cm, corresponding to a full output window equal to 9.2 cm. The average output power ranges from a value of $31.5\,\mathrm{MW}$ for the classic axial configuration, corresponding to a half-height of the output window equal to 7.6 cm, to a value up to $50\,\mathrm{MW}$ for the novel conical axial configuration for which the half-height of the exit window is equal to $4.6\,\mathrm{cm}$.
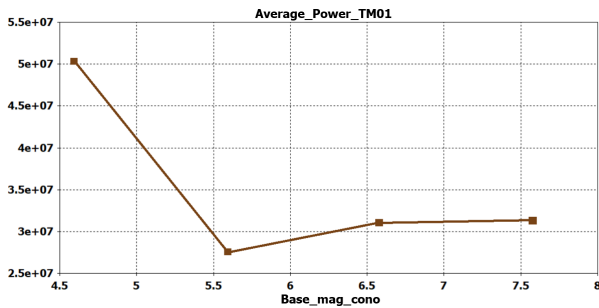
FIGURE 12. Average power vs. half-height output window aperture.

Figure 13 shows the parametric analysis for the cathode current value vs the half-height of the output window with the aperture varying from 4.6 cm to 7.6 cm.
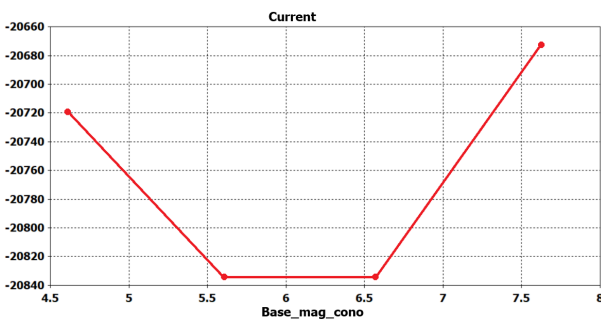
FIGURE 13. Cathode current vs. half-height output window aperture.

The optimum geometrical dimensions of the designed conical axial vircator are reported in Table II.

TABLE II. Geometrical dimensions of the added conical slices

Parameter	Quantity	Dimension
Length L of the cone slice	61.25	cm
Minimum distance d cone-slice	9.20	cm
Maximum distance D cone-slice	15.20	cm

Figure 14 shows the normed momentum for the novel conical axial Vircator configuration.
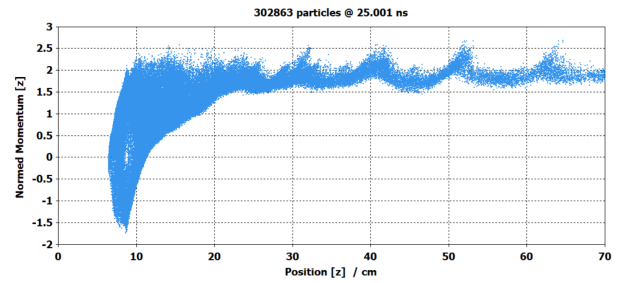
FIGURE 14. Normalized momentum for the conical axial geometry.

Figure 15 shows the peak output power waveform for the conic axial vircator with an output window aperture lower than the classical axial ones.
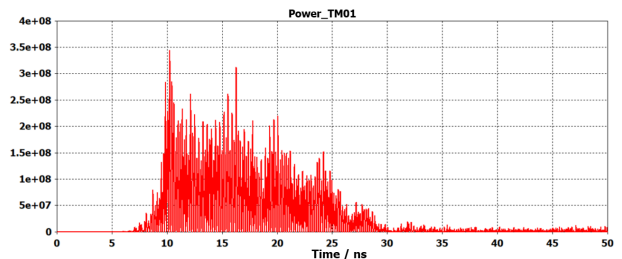
FIGURE 15. Output peak power vs time for the novel conic axial vircator geometry.

The novel geometrical structure allows for an increase in efficiency of more than $50\,\%$ compared to the classic structure.

Figure 16 shows the Fourier spectrum for the novel conical axial geometry. By comparing the simulation results of the novel proposed conical structure and classical structure, an increase in energy occurs.

The efficiency of the novel proposed cylindric waveguide with a conical structure inside reaches a value up to $60\,\%$ more than the classic cylindric waveguide, calculated according to [24]. The increase of $60\,\%$ in energy results from the integral over time of the output peak power waveform for the new Vircator, shown in Figure 16, compared to the integral of the output peak power waveform for to the traditional vircator shown in Figure 8. Moreover, it is not possible to reduce the diameter of the overall waveguide to have the interaction over the full length. Reducing the guide radius to a value of 4.6 cm, equal to the size of the half-height of the guide

at the end of the semi-cone, leads to an increase in the cut-off frequency of the guide for the TM_{01} mode used in the Vircator. In particular, for a value of the initial guide radius equal to 7.6 cm and a final radius of the cylindrical waveguide equal to 4.6 cm, the cut-off frequency for the TM_{01} mode shifts from 1.43 GHz to 2.36 GHz [23]. This value, very close to the working frequency of the device, does not allow the electromagnetic signal generation process. This is a very important result which, thanks to the novel solution, allows us to significantly increase the efficiency of the Vircator.
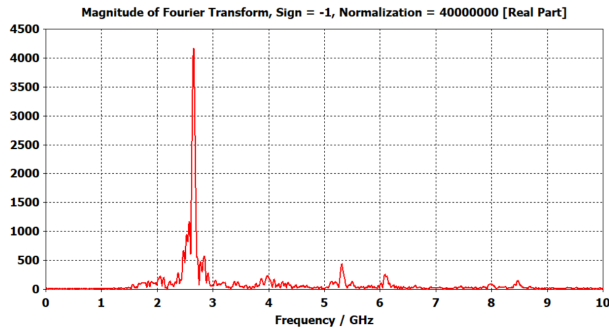

FIGURE 16. Fourier spectrum for the conic axial vircator.
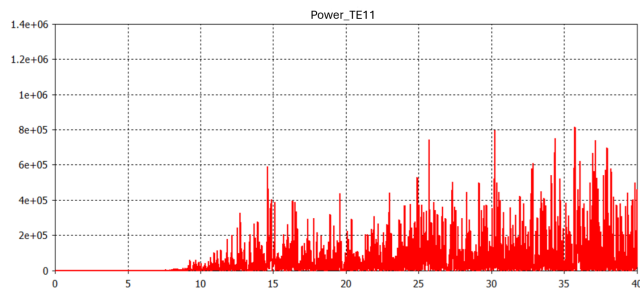

FIGURE 17. Output peak power vs. time for the TE11 mode of the conic geometry.

Figure 17 shows the graph of the output peak power for the TE_{11} mode for the novel conical axial geometry. By comparing Figure 9 and Figure 17, the output power for the TE_{11} mode for the classic vircator and the vircator with the conical insert, respectively, it can be noted that the amplitude of the TE_{11} mode for the vircator with the window aperture equal to 4.6 cm is smaller than the classic vircator with a half-size output window height equal to 7 cm. The half-height output window value equal to 4.6 cm is an optimum value in terms of high output power and allows a reduction of the TE_{11} mode. Figure 18 shows the wave particle transfer waveform for the conical vircator geometry. The novel geometry proposed in this article allows obtaining energy values for a single pulse of 60 % more than the energy value of a classic Vircator configuration. The spurious modes starting from the TE_{11} mode are more restricted for the axial Vircator based on the novel geometry.

The electrical parameters of the conical S-band vircator are reported in Table III. The novel axial geometry al-
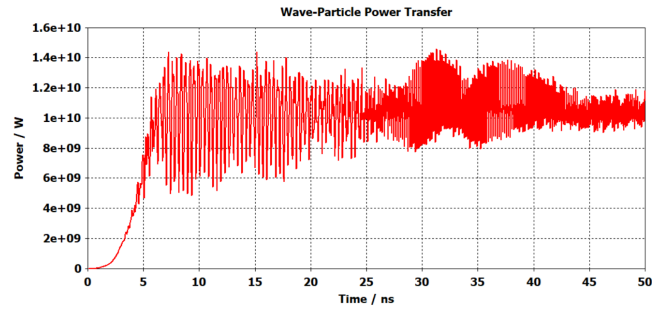

FIGURE 18. Wave particle transfer waveforms for the conical axial configuration.

lows obtaining better performance in terms of spectral purity, average output power, and high-efficiency, compared to the classical axial Vircator.

TABLE III. Electrical parameters for the conical S-band axial vircator

Parameter	Quantity	Dimension
Cathode voltage	520	kV
Beam Current	20.7	kA
Pulse width	50	ns
Average output power	50	MW
Pulse energy	2.0	J
Enhancement Efficiency	60	%

V. CONCLUSIONS

In this article, a novel conical axial vircator operating at S-band was presented. The integration of a conical structure in the cylindrical waveguide of an axial Vircator leverages the principles of Poynting's theorem to enhance the electric field intensity of the TM_{01} mode. This approach significantly improves the interaction with the virtual cathode, resulting in higher efficiency and power output for the Vircator. The novel axial vircator geometry proposed in this article allowed obtaining an increasing of the output power higher than 60 % compared to the output power of the classic axial vircator geometry. The novel structure was discussed for a single-stage axial vircator configuration consisting of a single virtual cathode. However, it could also be used for a multi-stage vircator structure proving very high efficiency and output power. The conical structure added into a circular waveguide paves the way to the application of the axial vircator for anti-drone applications [30], [31].

REFERENCES

[1] Benford, J., Swegle, J. A., and Schamiloglu, E., High Power Microwaves (CRC Press, 2015). https://doi.org/10.1201/b19681.

[2] A. V. Gaponov-Grekhov and V. L. Granatstein, Applications of High Power Microwaves. Norwood, MA, USA: Artech House, 1994.

[3] R. J. Barker and E. Schamiloglu, Eds., High-Power Microwave Sources and Technologies, Eds. New York, NY, USA: Wiley, 2001.

[4] S. H. Gold and G. S. Nusinovich, "Review of high-power microwave source research," Rev. Sci. Instrum., vol. 68, no. 11, pp. 3945–3974, 1997.

[5] D. J. Sullivan, "High power microwave generation from a virtual cathode oscillator (Vircator)," IEEE Trans. Nucl. Sci., vol. 30, no. 4, pp. 3426–3428, Aug. 1983.

IEEE Access

[6]   T. J. T. Kwan, "High-power coherent microwave generation from oscillating virtual cathodes," Phys. Fluids, vol. 27, no. 1, pp. 228–232, 1984.

[7]   W. Jiang, K. Masugata, and K. Yatsui, "Mechanism of microwave generation by virtual cathode oscillation," Phys. Plasmas, vol. 2, no. 3, pp. 982–986, 1995.

[8]   R. F. Hoeberling and M. V. Fazio, "Advances in virtual cathode microwave sources," IEEE Trans. Electromagn. Compat., vol. 34, no. 3, pp. 252–258, Aug. 1992.

[9]   A. E. Dubinov and V. D. Selemir, "Electronic devices with virtual cathodes (review)," J. Commun. Techn. Electr., vol. 47, no. 6, pp. 575–600, 2002.

[10]   V. D. Selemir, A. E. Dubinov, V. V. Voronin, and V. S. Zhdanov, "Key ideas and main milestones of research and development of microwave generators with virtual cathode in RFNC-VNIIEF," IEEE Trans. Plasma Sci., vol. 48, no. 6, pp. 1860–1867, Jun. 2020.

[11]   Alyokhin, B. V., Alexander E. Dubinov, V. D. Selemir, O. A. Shamro, K. V. Shibalko, N. V. Stepanov and V. E. Vatrunin. "Theoretical and experimental studies of virtual cathode microwave devices." IEEE Transactions on Plasma Science 22 (1994): 945-959.

[12]   Alyokhin, B. V., Alexander E. Dubinov, V. D. Selemir, O. A. Shamro, K. V. Shibalko, N. V. Stepanov and V. A. Tananakin. "HIGH EFFICIENCY PINCHING ELECTRON BEAM VIRCATOR." Ninth IEEE International Pulsed Power Conference 2 (1993): 703-.

[13]   Lipari Giuseppe, Paterna Giuseppe, Traina Eleonora, Muratore Antonino, Busacca Alessandro, Livreri Patrizia, Stivala Salvatore. (2023). Symmetric Vlasov-type antenna for High Power Microwave applications. 1-2. 10.1109/IVEC56627.2023.10157508. .

[14]   Patrizia Livreri, Francesco Bennardo, Benito Tusa, Pietro Bia, Marco Bartocci, Antonio Manna, Lorenzo Valletti, Franco Di Paolo and Ernesto Limiti "Efficiency Enhancement for an S-Band Axial Vircator Using 5-Stage Two-Step Tapered Radiators," 2022 23rd International Vacuum Electronics Conference (IVEC), Monterey, CA, USA, 2022, pp. 83-84, doi: 10.1109/IVEC53421.2022.10292221.

[15]   Valletti Lorenzo, Franco Di Paolo, Pietro Bia, Marco Bartocci, Antonio Manna, Patrizia Livreri and Ernesto Limiti. "High-Efficiency S-Band Axial Vircator." 2022 23rd International Vacuum Electronics Conference (IVEC) (2022): 97-98.

[16]   Valletti Lorenzo, Stefano Fantauzzi, Marco Bartocci, Pietro Bia, Antonio Manna, Patrizia Livreri, Franco Di Paolo and Ernesto Limiti. "Vircator Technologies Comparison and Novel Anode Analysis." 2021 Photonics Electromagnetics Research Symposium (PIERS) (2021): 2781-2789.

[17]   Sohail Mumtaz, Han Sup Uhm, Eun Ha Choi, "Progress in vircators towards high efficiency: Present state and future prospects", Physics Reports, Vol. 1069, 2024, Pages 1-46, ISSN 0370-1573, https://doi.org/10.1016/j.physrep.2024.03.003.

[18]   M. Sumathy, S. K. Chhotray, D. Senthil Kumar, K. S. Bhat and L. Kumar, "Analysis of a Multibeam Vircator Configuration for Efficiency Enhancement," in IEEE Trans. on Plasma Science, vol. 37, no. 2, pp. 293-297, Feb. 2009, doi: 10.1109/TPS.2008.918798.

[19]   S. Champeaux, P. Gouard, R. Cousin and J. Larour, "Improved Design of a Multistage Axial Vircator With Reflectors for Enhanced Performances," in IEEE Trans. on Plasma Science, vol. 44, no. 1, pp. 31-38, Jan. 2016, doi: 10.1109/TPS.2015.2502432.

[20]   S. Mumtaz, S. A. Munnaf and E. H. Choi, "Numerical study on the formation of second virtual cathode by using different material floating zone plate inside drift tube region," 2021 22nd International Vacuum Electronics Conference (IVEC), Rotterdam, Netherlands, 2021, pp. 1-2, doi: 10.1109/IVEC51707.2021.9722380.

[21]   S. Mumtaz and E. H. Choi, "An Efficient Vircator With High Output Power and Less Drifting Electron Loss by Forming Multivirtual Cathodes," in IEEE Electron Device Letters, vol. 43, no. 10, pp. 1756-1759, Oct. 2022, doi: 10.1109/LED.2022.3200395.

[22]   G. Migliore, A. Muratore, A. Busacca, P. Cusumano and S. Stivala, *"Novel Configuration for a C-Band Axial Vircator With High Output Power,"* in IEEE Transactions on Electron Devices, vol. 69, no. 8, pp. 4579-4585, Aug. 2022, doi: 10.1109/TED.2022.3184917

[23]   A. Roy, A. Sharma, S. Mitra, R. Menon, V. Sharma, K. V. Nagesh et al., "Oscillation frequency of a reflex-triode virtual cathode oscillator", IEEE Trans. Electron Devices, vol. 58, no. 2, pp. 553-561, Feb. 2011. DOI: 10.1109/TED.2010.2091132.

[24]   W. Jiang and M. Kristiansen, "Theory of the virtual cathode oscillator," Phys. Plasmas, vol. 8, no. 8, pp. 3781–3787, Aug. 2001, doi: 10.1063/1.1382643.

[25]   D. Sullivan, J. Walsh, and E. Coutsias, "Virtual cathode oscillator (vircator) theory," in High-Power Microwave Sources, V. Granatstein and I. Alexeff, Eds. Norwood, MA: Artech House, 1987, pp. 441–506.

[26]   W.Y.Woo, "Two-dimensional Features of Virtual Cathode and Microwave Emission" The Physics of Fluids, vol. 30, no. 1, pp. 239-244, January 1987. DOI: 10.1063/1.866181.

[27]   S. Ramo, J. R. Whinnery and T. Van Duzer, "Fields and Waves in Communication Electronics," Wiley, New York, 1965.

[28]   A. E. Dubinov and V. P. Tarakanov, "PIC simulation of a two-foil vircator," Laser Part. Beams, vol. 35, no. 2, pp. 362–365, Jun. 017.

[29]   A. E. Dubinov and V. P. Tarakanov, "Simulation of a magnetically isolated vircator with an under-limit electron beam," Plasma Phys. Rep., vol. 46, no. 5, pp. 570–573, May 2020.

[30]   H. Kang, J. Joung, J. Kim, J. Kang and Y. S. Cho, "Protect Your Sky: A Survey of Counter Unmanned Aerial Vehicle Systems," in IEEE Access, vol. 8, pp. 168671-168710, 2020, doi: 10.1109/ACCESS.2020.3023473

[31]   Park, S., Kim, H. T., Lee, S., Joo, H. & Kim, H. Survey on anti-drone systems: Components, designs, and challenges. IEEE Access 9, 42635–42659 (2021).

P. LIVRERI, IEEE Senior member, received the Laurea degree (Hons.) in electronics engineering, and the Ph.D. degree in electronics and communications engineering from the University of Palermo, Italy, in 1986 and 1992, respectively. From 1993 to 1994, she was a Researcher with the National Council for Researches, CNR, Rome, Italy. Since 1995, she has been serving as the Scientific Director for the Microwave Instruments and Measurements Laboratory' with the Department of Engineering, University of Palermo. In 2020, she also joined the CNIT National Laboratory for Radar and Surveillance Systems RaSS, Pisa. She is currently an Associate Professor with the Department of Engineering, University of Palermo, Italy, and a Visiting Professor with the San Diego State University, Department of Electrical and Computer Engineering, USA. She is a Principal Investigator of the "Microwave Quantum Radar" project, funded by the Ministry of Defense, in 2021. Her research interests include microwave and millimeter vacuum high power amplifiers (TWT, Klystron) and solid-state power amplifiers for radar applications; high power microwave sources (virtual cathode oscillator and magnetically insulated transmission line oscillator); microwave and optical antennas; and microwave quantum radar. Prof. Livreri is author or co-author of more than 200 publications on prestigious International Journals and Conferences.

●●●